

Novel synthesis of Pd nanoparticles for hydrogenation of biomass-derived platform chemicals showing enhanced catalytic performance†

Cite this: *RSC Adv.*, 2013, **3**, 25865

Kai Yan,^{*a} Cody Jarvis,^a Todd Lafleur,^a Yunxiang Qiao^b and Xianmei Xie^c

Robust Pd nanoparticles were novel and successfully synthesized on the γ -Al₂O₃ support by a simple and ecofriendly route through the assistance of CO₂. The unsupported and supported Pd nanoparticles were initially characterized with a combination of several techniques such as powder X-ray diffraction, energy-dispersion X-ray, X-ray photoelectron spectroscopy and transmission electron microscopy. The face-centered cubic Pd nanoparticles with uniform dispersion were successfully achieved with the Pd loading ranging from 1 wt% to 5 wt%. The resulting Pd nanoparticles (Pd/Al₂O₃) catalysts were found to be efficient and versatile for the hydrogenation of biomass-derived platform chemicals furfural and levulinic acid under very mild conditions, respectively, showing enhanced catalytic performance.

Received 15th July 2013
Accepted 14th October 2013

DOI: 10.1039/c3ra43619e

www.rsc.org/advances

1. Introduction

Metal nanoparticles with small size and uniform distribution exhibit interesting chemical and physical properties due to their attractive properties and high surface area.^{1,2} They have been widely used as catalysts in energy processing, fine chemical production, and air pollution control.^{3–5} For example, Pd nanoparticles have been utilized in the selective production of hydrogen from alcohols, Fischer–Tropsch synthesis, CO oxidation and NO_x reduction. The utilized metal nanoparticles are usually dispersed finely on a metal oxide support to prevent particle growth and aggregation, where the metal oxide support can enhance the surface area, light adsorption and charge-carrier separation.^{6,7} In the regard, γ -Al₂O₃ is perhaps the most often used and attractive support for metal nanoparticles catalysts because of its distinctive chemical, mechanical and thermal properties.⁸ On the other hand, the high surface area to volume ratio can lead to modifications in structure and properties. The uniform nanoparticle distributions will undoubtedly benefit the catalytic reaction.⁹

The Al₂O₃-supported Pd nanoparticles have been prepared by a variety of methods including molecular-capping-based colloidal synthesis,¹⁰ impregnation,¹¹ sonochemical method,¹² polyol reduction,¹³ and chemical fluid deposition method (CFD).^{14,15}

Among these different advanced methods, carbon dioxide (CO₂)-based CFD method appeared the most attractive due to the unique properties of CO₂. The environmentally benign CO₂ in its liquid or supercritical state (scCO₂) has a tremendous potential as a green reaction medium for the sustainable preparation of nanoparticles.^{16,17} The low surface tension of liquid CO₂ (from 4.5 dyn cm⁻¹ at 0 °C to zero at the critical point of 7.38 MPa at 31.1 °C) makes it as an excellent wetting agent.¹⁸

The supercritical CO₂-based CFD process often involves the dissolution of a metallic precursor in a supercritical fluid (scCO₂) and the exposure of the γ -Al₂O₃ support to the solution. After the adsorption of the precursor onto the support, the metallic precursor is converted to its metal form by the chemical or thermal reduction.¹⁸ Watkins *et al.*¹⁹ have done a lot of the pioneering work using scCO₂ and employed the resulting materials for semiconductor. Subsequently, monometallic Pd and Pt as well as bimetallic Pt–Cu, Pt–Ru, Pt–Au, Pt–Pd and Pt–Ni nanoparticles on carbon nanotubes were prepared by scCO₂ and the resultant nanoparticles were mainly employed for fuel cell.²⁰ Although the scCO₂ derived CFD method was advanced for the fabrication of metal nanoparticles, the employed supercritical fluid often associated with high temperature and high pressure, which often presented high requirement toward the reaction fixture and increasing the corresponding cost. Subsequently, the CFD method based on liquid carbon dioxide was more attractive. Kim *et al.*²¹ have done pioneering work using liquid CO₂ for the synthesis of supported metal catalysts. However, this method requires the high solubility of metal precursor inside the liquid CO₂. Besides, to the best of our knowledge, Pd nanoparticles on the γ -Al₂O₃ support and their enhanced catalytic properties for the hydrogenation of biomass-derived platform chemicals (furfural and levulinic

^aDepartment of chemistry, Lakehead University, 955 Oliver Road, Thunder Bay, ON P7B 5E1, Canada. E-mail: kyan@lakeheadu.ca; Tel: +1 807 627 3059

^bMax-Planck-Institut für Kohlenforschung, Kaiser-Wilhelm-Platz 1, 45470, Mülheim an der Ruhr, Germany

^cCollege of Chemistry and Chemical Engineering, Taiyuan University of Technology, 79 Yingze Street, 030024 Taiyuan, China

† Electronic supplementary information (ESI) available. See DOI: 10.1039/c3ra43619e

acid) have not been explored. Herein we describe a simple, green and scalable preparation strategy based on liquid CO₂ for the facile synthesis of Pd/Al₂O₃ nanoparticles catalyst and their enhanced performance for the versatile hydrogenation of biomass-derived platform chemicals (furfural and levulinic acid), where the value-added furfuryl alcohol and biofuel component γ -valerolactone was high selectively produced. The method developed in this work offered many advantages rather than the traditional impregnation method, including the minimization of liquid waste generation, avoiding the use of aqueous means, enhancing the environmental benignity, and rapid separation of final nanoparticles. Our results therefore provide an attractive approach for the preparation of high-performance nanoparticles catalysts in the processing of biomass.

2. Experimental section

2.1. Chemicals

γ -Al₂O₃ (surface-area of ~ 220 m² g⁻¹, Sigma-Aldrich), palladium(II) acetylacetonate [Pd(acac)₂, 99%, Sigma-Aldrich], furfural (99%, Alfa-Aesar), levulinic acid (98%, Alfa-Aesar), pentanoic acid ($\geq 99\%$, Sigma-Aldrich), 2-methyltetrahydrofuran (analytical standard, Sigma-Aldrich), 1,4-pentanediol (99%, Sigma-Aldrich), γ -valerolactone (99%, Sigma-Aldrich). All the chemicals were directly used without further treatment after purchase.

2.2. Catalysts preparations

A series of Pd nanoparticles were prepared using the palladium precursor (Pd(acac)₂) deposited on the γ -Al₂O₃ support as shown in Fig. 1, which was composed of three steps of impregnation, calcination and then reduction. The typical procedure was performed as following: firstly, a constant amount of γ -Al₂O₃ support (~ 0.3 g) and the precalculated amount of Pd(acac)₂ was added into a 50 mL vessel. After this, the vessel was sealed and filled with 18 g CO₂. The vessel was

under stirring condition for another 24 h to ensure the high dispersion of the Pd(acac)₂ at room temperature (RT). After this, the vessel was depressurized and the sample was calcinated at 450 °C for 3 h in the oven with air environment. In the end, the calcinated sample was pressurized with liquid CO₂ and reduced with H₂ at RT for 12 h under the stirring speed of 1000 rpm.

In comparative experiments, different Pd loading ranged from 1 wt% to 5 wt% were fabricated on the γ -Al₂O₃ support using the conventionally impregnation–reduction method. The typical procedure was performed as follows: firstly, a constant amount of γ -Al₂O₃ support (~ 0.3 g), 5 mL ethanol and the precalculated amount of Pd(acac)₂ was added into a 50 mL glass flask. After this, the flask was under the stirring speed of 1000 rpm for the impregnation of another 24 h at RT. After this step the sample was collected through the evaporation under 80 °C until the dry gel was formed. After this procedure, the sample was calcinated at 450 °C for 6 h in the oven with air environment, whereby organic compounds were burned and removed. Finally, the calcinated sample was reduced with 90% N₂–10% H₂ at 200 °C for 6 h. To verify the successful synthesis obtained, the typical characterizations (*e.g.*, XRD, EDX and XPS) of 5 wt% Pd/Al₂O₃ catalysts were shown in Fig. S1 (in the ESI†).

2.3. Catalysts characterizations

The Pd weight loading is expressed in wt% of Pd per gram of sample: Pd wt% = $m(\text{Pd}) \times 100\% / [m(\text{Pd}) + m(\gamma\text{-Al}_2\text{O}_3)]$. The powder X-ray diffraction (XRD) patterns for the crystal phase analysis were collected on Phillips PW 1050-3710 with Cu K α_1 of 1.54060 Å as a radiation source. The data were collected in the range of 10–90° 2 θ with a step width of 0.01°/2 θ . The particle size for each sample has been calculated from the Scherrer equation (1), where λ corresponds to the Cu K α radiation, and β is the full width at half-maximum for a reflection maximum located at 2 θ .

$$L = \frac{0.9\lambda}{\beta \cos \theta} \quad (1)$$

The textural feature and the composition of the resultant samples were examined by transmission electron microscopy (TEM) plus energy-dispersion X-ray (EDX) on a JEOL-2010 instrument. The mean particle size d was calculated from the following formula: $d = \sum n_i d_i / \sum n_i$, where n_i is the number of particles of size d_i . The detection limit is about 1 nm for the supported Pd particles.

X-ray photoelectron spectroscopy (XPS) measurements were performed with an ESCALAB 250 spectrometer with a hemispherical analyzer and a monochromatized Al K α X-ray source ($E = 1486.6$ eV), operated at 15 kV and 15 mA. For the narrow scans, analyzer pass energy of 40 eV was applied. The hybrid mode was used as lens mode.

The reducibility of the calcined samples was determined by H₂-temperature-programmed reduction (TPR). In these measurements, 50 mg of a sample was placed in a quartz reactor and heated at 10 °C min⁻¹ up to 550 °C under a He flow of 20 mL min⁻¹, and held at this temperature for 1 h. The reactor was then cooled down to 0 °C and the sample exposed to a

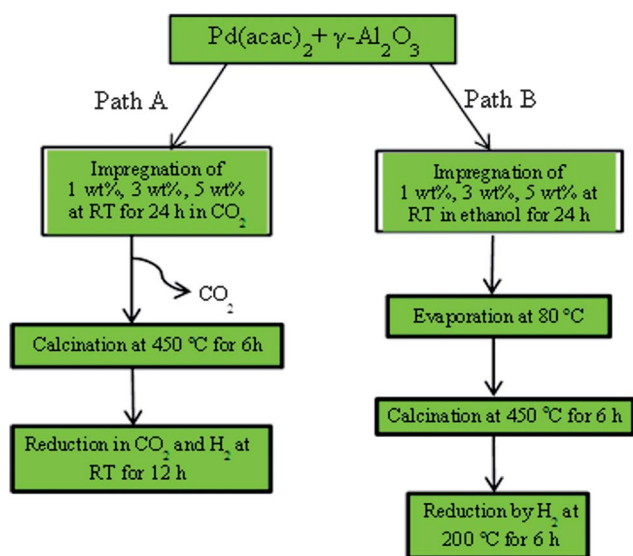


Fig. 1 Schematic diagram for the synthesis of Pd nanoparticles on the γ -Al₂O₃ support.

stream of 5% H₂/Ar at a flow rate of 20 mL min⁻¹. Subsequently, the sample was heated up to 400 °C at a heating rate of 10 °C min⁻¹. The amount of hydrogen consumed as a function of temperature was monitored on-line on a TCD detector. The maximum rate of H₂ consumption was used to choose the reduction temperature for each catalyst to be conducted *in situ* before reaction.

2.4. Liquid-phase hydrogenation of furfural

The liquid-phase hydrogenation of furfural was performed in a 20 mL vessel (Parr Company). 2.0 mL furfural was added into 5 mL octane, followed by the addition of 0.1 g catalyst into the solution under the continuous stirring speed of 1000 rpm. The vessel was flushed with argon to remove the inside air and then H₂ was input. After reaction, the vessel was cooled down to room temperature in a controlled manner using a water bath. The product mixture was firstly centrifuged for 30 min, and then filtrated, followed by a second filtration and dilution by dichloromethane. The subsequent samples were analyzed by GC (Shimadzu 2014, column: 30 m SE-54 G/17, FID). The column temperature was raised from 40 to 250 °C with a heating rate of 5 °C min⁻¹. The injector temperature was 350 °C, which was loaded with a sampling volume of 1 μL.

2.5. Hydrogenation of levulinic acid

The hydrogenation of levulinic acid was performed in a 25 mL vessel (Parr Company) with the external temperature and pressure controller. Typically, constant amount of LA was dissolved in deionized water (5 mL) and the catalyst was added into the solution. After reactions, the vessel was cooled down by water with temperature controller. The reaction products were firstly centrifuged for 30 min and then filtrated to obtain clear solution. The samples were analysed by GC (Shimadzu 2014, column: 30 m DBWaxetr, FID detector; the column temperature was raised from 40 °C to 250 °C with a heating rate of 3 °C min⁻¹; the injector temperature was set at 350 °C with a heating speed of 10 °C min⁻¹ and the sampling volume was 0.2 μL).

3. Results and discussions

3.1. Catalyst characterizations

After the reduction by H₂ in CO₂ at room temperature, the Pd nanoparticles will be obtained simply through the releasing of H₂ and CO₂. In combination with the economic view, the highest Pd loading was limited to 5 wt%. The crystal structure of the γ-Al₂O₃ support and the supported nanoparticles were initially studied by Powder X-ray diffraction patterns as shown in Fig. 2. Three distinct reflections of γ-Al₂O₃ (Fig. 2a) with 2θ indexed at ~37° (311), ~46° (400) and ~67° (440). The analysis shows the average crystallite size of γ-Al₂O₃ based on (440) to be approximately 10 nm according to Scherrer equation. Other weak diffraction peaks (the inserted scale-up diffraction pattern in Fig. 2) indexed at ~21° (111), ~29° (220), ~40° (222), ~61° (511) and ~85° (444). Overall, all these diffraction peaks are in well agreement with the standard card of γ-Al₂O₃ (JCPDS card, file no. 00-001-1308). At the low loading of 1 wt% (Fig. 2b),

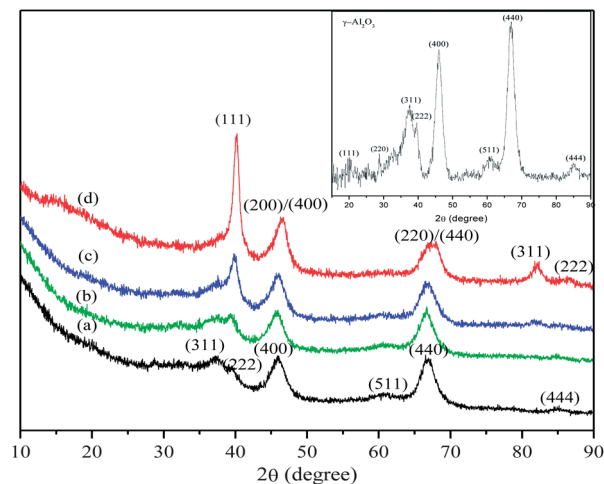


Fig. 2 XRD analysis of the (a) γ-Al₂O₃ support; (b) 1 wt%; (c) 3 wt%; (d) 5 wt% Pd/Al₂O₃ nanoparticles.

nearly the same diffraction pattern was obtained as of γ-Al₂O₃, only the peak indexed at ~40° (222) was slightly increased. Meanwhile, the peaks indexed at ~46° (400) and ~67° (440) seem to decrease some of extent in comparison with the diffraction pattern of γ-Al₂O₃. With the Pd loading increasing to 5 wt% (Fig. 2d), the diffraction pattern indexed as 2θ at ~40°

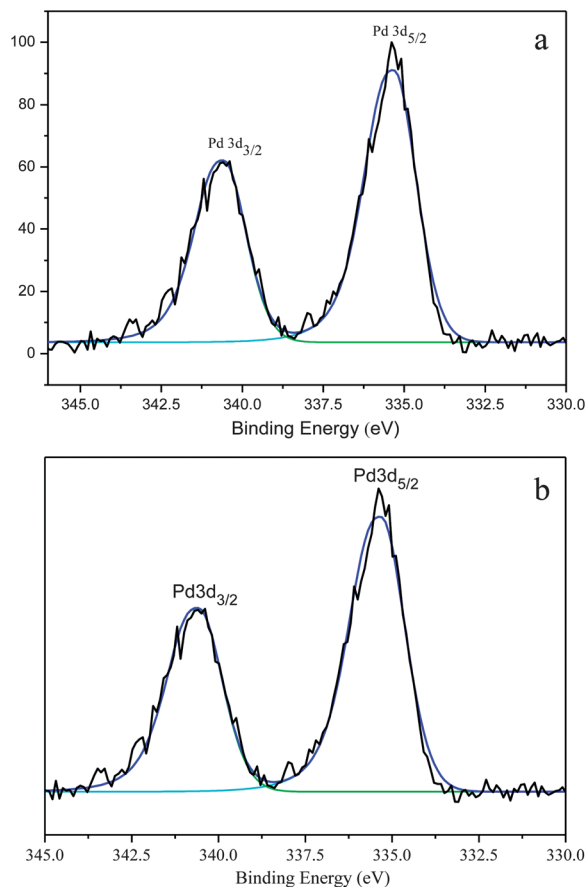


Fig. 3 XPS analysis of the (a) 3 wt% and (b) 5 wt% Pd/Al₂O₃.

(111), $\sim 46^\circ$ (200), $\sim 82^\circ$ (311) identified as single hexagonal fcc phase of Pd, although the diffraction peaks at $\sim 46^\circ$ of the crystal facet (400) in the γ -Al₂O₃ support and (200) of Pd overlapped some of extent. Additionally, small crystal sizes of ~ 6.3 and ~ 7.5 nm were obtained in the 3 wt% and 5 wt% loading based on the Scherrer equation, respectively, which were close to the size calculated from TEM images (Fig. 4c and d).

For the successful synthesis of metal nanoparticle catalysts, the oxidation state of the surface metal in the sample was very sensitive towards their catalytic activities. Thus XPS measurements were initially employed to study the oxidation state and the representative analysis results of the selected 3 wt% Pd/Al₂O₃ and 5 wt% Pd/Al₂O₃ were shown in Fig. 3. It was

interesting to find the presence of two prominent sets of Pd (3d) peaks, corresponding to the 3d_{3/2} via 3d_{5/2} orbital states, which demonstrated that Pd was present on the surface in the reduced state. The peak regions of metal Pd could be fitted with two sets of peaks at 340.6 eV (3d_{3/2}) and 335.3 eV (3d_{5/2}), indicating that the fresh catalysts contained Pd⁰ centers in the samples.²¹ Besides, the very weak peak was observed at 341.7 eV and 336.5 eV, which was possible due to the presence of very small amount of PdO on the surface or the interaction between of Pd and the oxygen from the Al₂O₃ support.²²

The textural structure and the size distribution of the resultant Pd nanoparticles often display important influence on their catalytic activities, TEM was further employed. The TEM images and the Pd particles size distribution were shown in Fig. 4. TEM image of the support γ -Al₂O₃ revealed three broad diffraction rings corresponding to the (311), (400) and (440) reflections (Fig. 4a and b) and these *d*-spacings are consistent with the γ -alumina structure.²³ Besides, the TEM images of the γ -Al₂O₃ support (Fig. 4a and b) show the enhanced surface contrast on facets that terminate with (111) planes (*d*₁₁₁ = 0.2003 nm) and (100) planes at the end of the edges.²³ The ordered lattice fringes dominated the texture of the γ -Al₂O₃ support, which would be beneficial for enhancing the dispersion of fine Pd nanoparticles in the sample.^{23,24} TEM images of Pd/Al₂O₃ nanoparticles exhibited that the uniform and small size of Pd particles were highly distributed on γ -Al₂O₃ support (Fig. 4c and d). Besides, the introduction of Pd on γ -Al₂O₃ support did not change the structure of γ -Al₂O₃. The slightly unavoidable aggregation of Pd nanoparticle was found and only few bigger particles were observed in a few areas (Fig. 4c and d). Small Pd nanoparticles with a mean size of 6.20 nm (Fig. 4e) and 7.34 nm (Fig. 4f) in the case of 3 wt% and 5 wt% loading, respectively, appeared as a high dispersion in the material. To ascertain whether the metal nanoparticles existed on the surfaces, EDX analysis further adopted and the spectrum of the support Al₂O₃ and 5 wt% Pd/Al₂O₃ were shown in Fig. 4g and h, respectively. EDX analysis spectra (Fig. 4h) presents the peaks of Pd, Al and O where they should be. It clearly presented the peaks where Pd and Al should be, which confirmed the existence of Pd in the resulting samples. Besides, no distinct difference of Pd amount was revealed by the EDX analysis in several different areas, indicating the uniform dispersion of Pd nanoparticles in the sample.

The H₂-TPR profiles of the chosen 3% Pd/Al₂O₃ catalysts prepared by the CO₂-assisted method and 3% Pd/Al₂O₃ catalysts synthesized by the traditional impregnation method, are compared in Fig. S2.† For 3% Pd/Al₂O₃ prepared by CO₂-assisted method, the TPR profile (Fig. S2a†) mainly exhibits one peak centered on $\sim 95^\circ\text{C}$, indicative of the H₂ consumption.^{25a} The H₂ profile was consistent with the decomposition of (Pd(acac)₂), which was reported to form at room temperature over large Pd particles.^{25b} Besides, a second broader peak was detected in the range of 200 to 300 °C, which was due to the water evolution.^{25c,d}

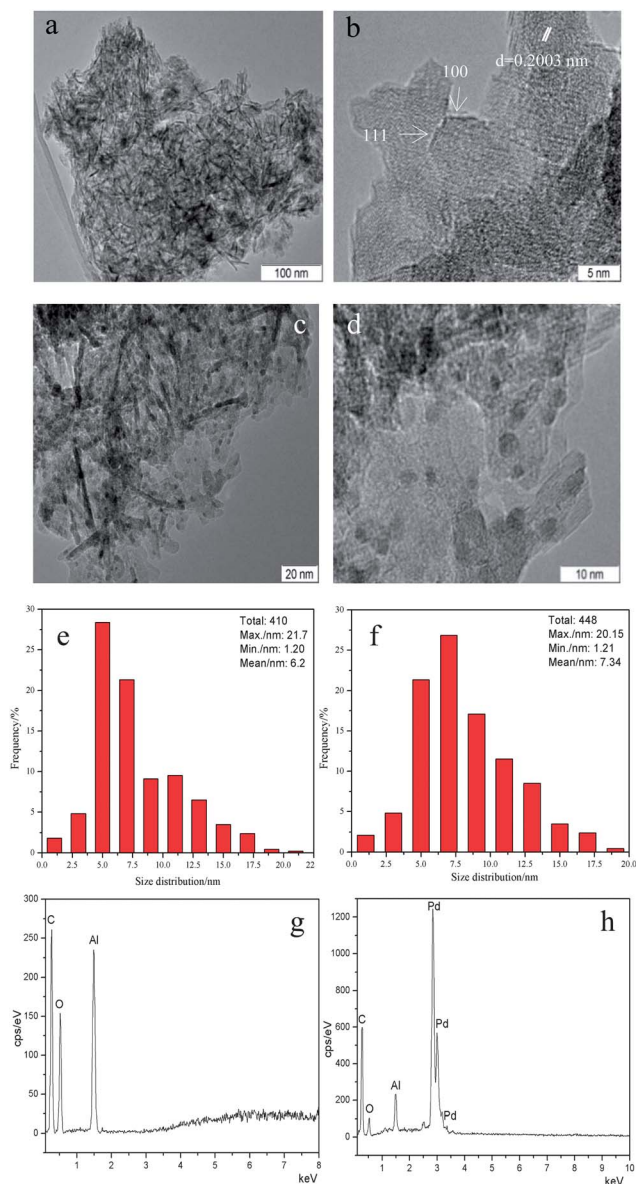


Fig. 4 TEM images, size distribution and EDX spectrum of the γ -Al₂O₃ support and the Pd nanoparticles catalysts: (a and b) TEM image of γ -Al₂O₃; (c) TEM image of 3 wt% Pd/Al₂O₃; (d) TEM image of 5 wt% Pd/Al₂O₃; (e) size distribution of 3 wt% Pd/Al₂O₃; (f) size distribution of 5 wt% Pd/Al₂O₃; (g) EDX spectrum of γ -Al₂O₃; (h) EDX spectrum of 5 wt% Pd/Al₂O₃.

3.2. Hydrogenation of furfural

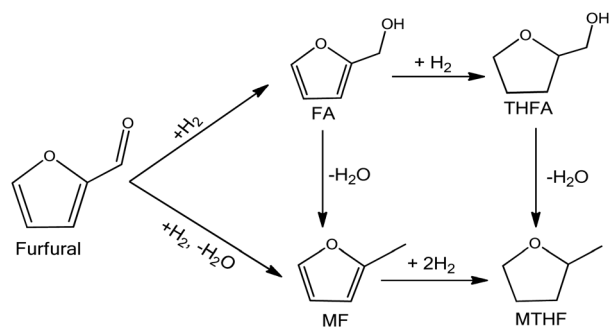
The resulting Pd/Al₂O₃ nanoparticles catalysts were employed for the liquid-phase hydrogenation of furfural (Scheme 1). The

catalytic results of the γ -Al₂O₃ support and a series of Pd/Al₂O₃ nanoparticles catalysts are presented in Table 1. The turnover number (TON), defined as the moles of converted furfural molecules per mole of noble metal atoms on the γ -Al₂O₃ support, was used to compare the overall catalytic performances (Table 1). Overall, the synthesized Pd/Al₂O₃ nanoparticles catalysts display good performance in the liquid-phase hydrogenation of furfural. First, it was found that the main product was furfuryl alcohol coming from the hydrogenation of the C=O bond (no. 1 to no. 5). In addition to the main products, there are several compounds derived from side reactions (*i.e.* the hydrogenation of the furan ring to tetrahydrofurfuryl alcohol (THFA), hydrogenolysis of the C=O bond to MF, decarbonylation to furan and further hydrogenation to THF).^{26,27} Among the side products, only a few amounts of furan and THF were observed by GC. Second, in the comparative reaction using the support γ -Al₂O₃ as catalyst (no. 1), \sim 5.1% conversion of furfural was obtained and nearly no detectable product was found. Increasing the Pd loading from 1 wt% to 5 wt% (no. 1 to no. 4), the conversion of furfural was increased stably from 21.2% to 39.4% and the TONs vary from 492 (no. 2) to 172 (no. 4). The highest selectivity of FA was obtained with 89.1% selectivity and a TON of 205 at 26.9% conversion of furfural using the 3 wt% Pd/Al₂O₃ nanoparticle catalyst (no. 3). Additionally, \sim 8%

selectivity of THFA and \sim 2% selectivity of MF were simultaneously obtained. With the Pd loading increasing to 5 wt%, 84.9% selectivity of FA with the TON of 172 was achieved at 39.4% conversion was achieved (no. 4). Meanwhile, \sim 14% selectivity of THFA and \sim 1% selectivity of MF were produced. These results confirmed that the Pd loading can be used to alter the extent of hydrogenation, where the small particle sizes of Pd with high surface areas would play an important role in enhancing the mass transportation and alternatively influence the catalytic activities importantly.²⁸ On the other hand, for hydrogen adsorption on transition metals, it is often considered that the electron is donated from the σ -bond of hydrogen to the d-band of Pd, where the d-band centre in the surface electronic structure may also play a role.²⁹ Third, the Pd/Al₂O₃ nanoparticle catalysts were synthesized by the traditional impregnation method and exhibited lower performances in the hydrogenation of furfural. For example, the 5 wt% Pd/Al₂O₃ nanoparticles catalysts display 91.6% selectivity of FA with the TON of 120 at 28.7% conversion of furfural (no. 7). A complete understanding of the reaction parameters deserves future attention. However, our facile approach for the preparation of metal nanoparticles will be of great potential for various important reactions in the processing of biomass.

3.3. Hydrogenation of levulinic acid

The robust Pd/Al₂O₃ nanoparticles were further employed for the hydrogenation of biomass-derived levulinic acid (LA) as shown in Scheme 2 and the catalytic results are shown in Table 2. In the hydrogenation of LA, the γ -valerolactone (GVL) was more preferred to be produced due to its negative Gibbs free energy ($\Delta G^\circ = -22 \text{ kJ mol}^{-1}$) in principle.³⁰ However, the easily occurred side reactions (*e.g.*, further hydrogenation of GVL to 2-methyltetrahydrofuran (MTHF), dehydration of the intermediate 4-hydroxypentanoic acid and then further hydrogenated to pentanoic acid (PA)) would influence the production of GVL in a significant manner.^{30,31} In this work, it was clear to find that the synthesized Pd/Al₂O₃ nanoparticles catalysts continue to display very good performance, where over 94% selectivity of GVL was achieved when the Pd/Al₂O₃ nanoparticles catalyst was employed. Additionally, the metal Pd loading presented crucial influence on the catalytic activities. First, increasing the Pd loading from 1 wt% to 5 wt% (no. 1 to no. 5), the conversion of LA increased clearly from 31.2% to 63.5%. When 1 wt% Pd/Al₂O₃ nanoparticle catalyst was employed (no. 1), 94.3% selectivity of GVL and 5.0% selectivity of PA was observed at

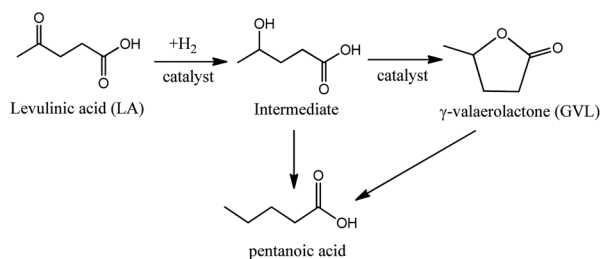


Scheme 1 Hydrogenation of furfural to value-added chemicals.

Table 1 Catalytic performance of the support γ -Al₂O₃ and the Pd/Al₂O₃ catalysts in the hydrogenation of furfural^a

No.	Catalyst ^b	Conv./%	S(FA)/%	S(THFA)/%	S(MF)/%	TON ^c
1	0 wt%	5.1	<0.1	<0.1	<0.1	—
2	1 wt%	21.2	90.3	6.5	1.4	491.8
3	3 wt%	26.9	89.1	7.6	1.5	205.3
4	5 wt%	39.4	84.9	13.8	0.9	171.9
5 ^d	1 wt%	10.9	87.5	7.2	0.7	—
6	3 wt%	20.1	90.2	5.2	1.0	—
7	5 wt%	28.7	81.6	15.8	1.2	120.4

^a Reaction conditions: $V(\text{furfural}) = 2 \text{ mL}$, $V(\text{octane}) = 5 \text{ mL}$, $m(\text{catalyst}) = 0.1 \text{ g}$, $p(\text{H}_2) = 45 \text{ bar}$, $T = 150 \text{ }^\circ\text{C}$, stirring speed = 1000 rpm. Conv.: the conversion of furfural, S(FA): the selectivity of furfuryl alcohol, S(THFA): the selectivity of tetrahydrofurfuryl alcohol (THFA), S(MF): selectivity of 2-methylfuran (MF). ^b Catalyst was Pd/Al₂O₃. ^c TON was calculated according to FA. Turnover numbers (TON) = the molar of the desired product/the molar the catalyst used. ^d 1 wt% (No. 5) to 5 wt% Pd/Al₂O₃ (No. 7) was prepared by the traditional impregnation method.



Scheme 2 Hydrogenation of LA to value-added chemicals.

Table 2 Catalytic performance of the Pd/Al₂O₃ nanoparticle catalysts in the hydrogenation of levulinic acid^a

No.	Catalyst	Conv./%	S(GVL)/%	S(PA)/%	TON ^b
1	1 wt%	31.2	94.3	5.0	1361.7
2	3 wt%	48.7	95.0	4.6	713.8
3	5 wt%	63.2	96.3	3.7	565.2
4 ^c	5 wt%-Im	52.9	95.2	4.5	473.2

^a Hydrogenation conditions: $m(\text{LA}) = 5.05 \text{ g}$, $V(\text{H}_2\text{O}) = 5 \text{ mL}$, $p(\text{H}_2) = 45 \text{ bar}$, $T = 160 \text{ }^\circ\text{C}$, $t = 6 \text{ h}$, $m(\text{catalyst}) = 0.10 \text{ g}$, stirring speed = 1000 rpm. Conv.: the conversion of levulinic acid, S(GVL): the selectivity of γ -valerolactone, S(PA): the selectivity of pentanoic acid. ^b TON was calculated according to GVL. Turnover numbers (TON) = the molar of the desired product/the molar the catalyst used. ^c 5 wt% Pd/Al₂O₃ was prepared by the impregnation method.

31.2% conversion of LA. Meanwhile, few amounts (less than 1%) of MTHF were detected by GC. With the loading increasing to 5 wt%, 96.3% selectivity of GVL and 3.7% selectivity of PA was achieved at 63.2% conversion (no. 3). These data suggested that the Pd loading can be used to alter the extent of hydrogenation, whereas the uniform Pd nanoparticles with small size (Fig. 4) would play a role.²⁷ Second, the TON vary from 1362 (no. 1) to 565 (no. 3). A 3 wt% loading of Pd/Al₂O₃ generally lead to higher TONs than the loading of 5 wt%. This is because the metal nanoparticles are generally smaller at lower loadings, as evidenced by TEM (Fig. 4). Third, in comparison, the 5 wt% Pd/Al₂O₃ nanoparticle catalysts prepared by the impregnation method displayed that 95.2% selectivity of GVL with the TON of 473, and 4.5% selectivity of PA was achieved at 52.9% conversion of LA, which further confirmed that the method developed in this work is superior. Future work need focus on the improvement of the catalytic performance through the optimization of reaction parameters. However, the method developed in this work using liquid CO₂ often offer many advantages rather than the traditional impregnation methods, including the minimization of liquid waste generation, avoiding the use of organic solvents, enhancing the environmental benignity, a high rate of mass transfer, and rapid separation of products.

4. Conclusions

In this work, robust Pd nanoparticle was successfully fabricated on the support γ -Al₂O₃ through the assistance of the green solvent CO₂. Through using this novel method, it offers the minimization of liquid waste generation, avoiding the use of organic solvents and rapid separation of the final nanoparticles. The synthesized Pd/Al₂O₃ nanoparticles catalysts exhibit the enhanced catalytic performance for the hydrogenation of biomass-derived platform chemical furfural and levulinic acid in comparison with the Pd/Al₂O₃ nanoparticles catalysts prepared by the traditional method. In the first liquid-phase hydrogenation of furfural, furfuryl alcohol (84.9% selectivity and TON of 172) was produced on the 5 wt% Pd/Al₂O₃ nanoparticle catalyst under mild reaction condition

of 140 °C. The Pd/Al₂O₃ nanoparticles catalysts were also efficient for the hydrogenation of biomass-derived levulinic acid, where over 94% selectivity of the promising biofuel component γ -valerolactone was achieved in the presence of Pd/Al₂O₃ catalysts. 94.3% selectivity of γ -valerolactone with the TON of 1362 was obtained for the conversion of levulinic acid. A complete work of optimization of the reaction parameters would benefit for our understanding of the reaction mechanism and deserved our future attention. However, the current work confirmed that the synthesis strategy to fabricate Pd nanoparticles on the γ -Al₂O₃ support was attractive and the developed catalyst may be a good candidate for industrially important chemical reactions.

Notes and references

- (a) M. Sankar, N. Dimitratos, P. J. Miedziak, P. P. Wells, C. J. Kielye and G. J. Hutchings, *Chem. Soc. Rev.*, 2012, **41**, 8099; (b) H. M. T. Galvis, J. H. Bitter, C. B. Khare, M. Ruitenbeek, A. I. Dugulan and K. P. de Jong, *Science*, 2012, **335**, 835.
- (a) L. Hu, G. Zhao, W. Hao, X. Tang, Y. Sun, L. Lin and S. J. Liu, *RSC Adv.*, 2012, **2**, 11184; (b) K. Yan, T. Lafleur and J. Y. Liao, *J. Nanopart. Res.*, 2013, **15**, 1906; (c) Y. B. Huang, Z. Yang, J. Dai, Q. Guo and Y. Fu, *RSC Adv.*, 2012, **2**, 11211.
- P. Herves, M. Perez-Lorenzo, L. M. Liz-Marzan, J. Dzubiella, Y. Lu and M. Ballauff, *Chem. Soc. Rev.*, 2012, **41**, 5577.
- (a) Y. M. Lu, H. Z. Zhu, W. G. Li, B. Hu and S. H. Yu, *J. Mater. Chem. A*, 2013, **1**, 3783; (b) J. Kou and R. S. Varma, *RSC Adv.*, 2012, **2**, 10283; (c) M. Zahmakiran and S. Ozkar, *Nanoscale*, 2011, **3**, 3462.
- Y. X. Qiao, H. Li, L. Hua, L. Orzechowski, K. Yan, B. Feng, Z. Y. Pan, N. Theyssen, W. Leitner and Z. S. Hou, *ChemPlusChem*, 2012, **77**, 1128.
- (a) Y. Zheng, Y. Jiao, M. Jaroniec, Y. G. Jin and S. Z. Qiao, *Small*, 2012, **8**, 3550; (b) A. Z. Moshfegh, *J. Phys. D: Appl. Phys.*, 2009, **42**, 233001.
- J. H. Kim, J. S. Park, H. W. Chung, B. W. Boote and T. R. Lee, *RSC Adv.*, 2012, **2**, 3968.
- Y. Rozita, R. Brydson and A. J. Scott, *J. Phys.: Conf. Ser.*, 2010, **241**, 012096.
- H. U. Blaser, A. Indolese, A. Schnyder, H. Steiner and M. Studer, *J. Mol. Catal. A: Chem.*, 2001, **173**, 3.
- P. D. Burton, T. J. Boyle and A. K. Datye, *J. Catal.*, 2011, **280**, 145.
- K. Persson, P. O. Thevenin, K. Jansson, J. Agrell, S. G. Järås and L. J. Pettersson, *Appl. Catal., A*, 2003, **249**, 165.
- K. Okitsu, Sonochemical Synthesis of Metal Nanoparticles, in *Theoretical and Experimental Sonochemistry Involving Inorganic Systems*, ed. P. M. Ashokkumar, Springer, 2011, pp. 131–148.
- X. Xu, Y. Li, Y. T. Gong, P. F. Zhang, H. R. Li and Y. Wang, *J. Am. Chem. Soc.*, 2012, **134**, 16987.
- (a) X. R. Ye, Y. H. Lin, C. M. Wang, M. H. Engelhard, Y. Wang and C. M. Wai, *J. Mater. Chem.*, 2004, **14**, 908; (b) K. Yan, T. Lafleur, J. Y. Liao and X. M. Xie, *Sci. Adv. Mater.*, 2014,

- 6, 1; (c) Y. Zhang and C. Erkey, *J. Supercrit. Fluids*, 2006, **38**, 252.
- 15 J. Kim, M. J. Kelly, H. H. Lam, G. W. Roberts and D. J. Kiserow, *J. Phys. Chem. C*, 2008, **112**, 10446.
- 16 (a) J. Kim, G. W. Roberts and D. J. Kiserow, *Chem. Mater.*, 2006, **18**, 4710; (b) Z. Hou, N. Theyssen and W. Leitner, *Green Chem.*, 2007, **9**, 127.
- 17 (a) E. J. Beckman, *J. Supercrit. Fluids*, 2004, **28**, 121; (b) W. Leitner, *Acc. Chem. Res.*, 2002, **35**, 746.
- 18 (a) P. G. Jessop, S. M. Mercer and D. J. Heldebrant, *Energy Environ. Sci.*, 2012, **5**, 7240; (b) A. E. Charles, C. L. Liotta, D. Bush, J. S. Brown and J. P. Hallett, *J. Phys. Chem. B*, 2004, **108**, 18108; (c) Y. Zhang, D. F. Kang, M. Aindow and C. Erkey, *J. Phys. Chem. B*, 2005, **109**, 2617.
- 19 (a) E. T. Hunde and J. J. Watkins, *Chem. Mater.*, 2004, **16**, 498; (b) D. P. Long, J. M. Blackburn and J. J. Watkins, *Adv. Mater.*, 2000, **12**, 913; (c) A. H. Romang and J. J. Watkins, *Chem. Rev.*, 2010, **110**, 459.
- 20 (a) C. H. Yen, K. Shimizu, Y. Y. Lin, F. Bailey, I. F. Cheng and C. M. Wai, *Energy Fuels*, 2007, **21**, 2268; (b) S. E. Bozbag and C. Erkey, *J. Supercrit. Fluids*, 2012, **62**, 1; (c) C. Erkey, *J. Supercrit. Fluids*, 2000, **17**, 259.
- 21 (a) Y. J. Han, J. M. Kim and G. D. Stucky, *Chem. Mater.*, 2000, **12**, 2068; (b) M. Kelly, J. Kim, G. Roberts and H. Lamb, *Top. Catal.*, 2008, **49**, 178; (c) K. Yan, T. Lafleura, G. S. Wu, J. Y. Liao, C. Ceng and X. M. Xie, *Appl. Catal., A*, 2013, **468**, 52; (d) W. S. Liao, Y. Takeshita and C. M. Wai, *Appl. Catal., B*, 2009, **88**, 173.
- 22 M. Flytzani-Stephanopoulos and B. C. Gates, *Annu. Rev. Chem. Biomol. Eng.*, 2011, **3**, 545; A. F. Gusovius, T. C. Watling and R. Prins, *Appl. Catal., A*, 1999, **188**, 187.
- 23 D. A. Jefferson, *Philos. Trans. R. Soc. London, Ser. A*, 2000, **358**, 2683.
- 24 G. R. Lovely, A. P. Brown, R. Brydson, A. I. Kirkland, R. R. Meyer, L. Chang, D. A. Jefferson, M. Falke and A. Bleloch, *Appl. Phys. Lett.*, 2006, **88**, 93124.
- 25 (a) A. B. Gaspar and L. C. Dieguez, *Appl. Catal., A*, 2000, **201**, 241; (b) S. Fessi, A. S. Mamede, A. Ghorbel and A. Rives, *Catal. Commun.*, 2012, **27**, 109; (c) Y. Cao, R. Ran, X. Wu, B. Zhao, J. Wan and D. Weng, *Appl. Catal., A*, 2013, **457**, 52; (d) J. J. Panpranot, O. Tangjitwattakorn, P. Praserttham and J. G. Goodwin Jr, *Appl. Catal., A*, 2005, **292**, 322.
- 26 (a) K. Yan, J. Y. Liao, X. Wu and X. M. Xie, *RSC Adv.*, 2013, **3**, 3853; (b) K. Yan, X. Wu, X. An and X. M. Xie, *Funct. Mater. Lett.*, 2013, **6**, 1350007; (c) S. Sitthisa, T. Pham, T. Prasomsri, T. Sooknoi, R. G. Mallinson and D. E. Resasco, *J. Catal.*, 2011, **280**, 17.
- 27 (a) H. Y. Zheng, Y. L. Zhua, B. T. Teng, Z. Q. Bai, C. H. Zhang, H. W. Xiang and Y. W. Li, *J. Mol. Catal. A: Chem.*, 2006, **246**, 18; (b) J. P. Lange, E. Heide, J. van Buijtenen and R. Price, *ChemSusChem*, 2012, **5**, 150; (c) S. Dutta, *RSC Adv.*, 2012, **2**, 12575.
- 28 (a) R. Rao, A. Dandekar, R. T. K. Baker and M. A. Vannice, *J. Catal.*, 1997, **171**, 406; (b) P. Mäki-Arvela and D. Y. Murzin, *Appl. Catal., A*, 2013, **451**, 251.
- 29 (a) V. Pallassana, M. Neurock, L. B. Hansen, B. Hammer and J. K. Nørskov, *Phys. Rev. B: Condens. Matter Mater. Phys.*, 1999, **60**, 6146; (b) J. K. Nørskov, F. Abild-Pedersen, F. Studt and T. Bligaard, *Proc. Natl. Acad. Sci. U. S. A.*, 2011, **108**, 937.
- 30 J. C. Serrano-Ruiz, R. M. West and J. A. Dumesic, *Annu. Rev. Chem. Biomol. Eng.*, 2010, **1**, 79.
- 31 (a) C. E. Chan-Thaw, M. Marelli, R. Psaro, N. Ravasio and F. Zaccheria, *RSC Adv.*, 2013, **3**, 1302; (b) A. M. R. Galletti, C. Antonetti, V. De Luise and M. Martinelli, *Green Chem.*, 2012, **14**, 688.